Confined H_2O molecules as local probes of pressure-induced amorphisation in faujasite

Jadna Catafesta, Frederico Alabarse, Claire Levelut, Aude Isambert, Philippe Hébert, Shinji Kohara, David Maurin, Jean-Louis Bantignies, Olivier Cambon, Gaëlle Creff, et al.

Confined H_2O molecules as local probes of pressure-induced amorphisation in faujasite

Jadna Catafesta,†[ab] Frederico Alabarse,‡[a] Claire Levelut,[b] Aude Isambert,§[c] Philippe Hébert,[c] Shinji Kohara,[d] David Maurin,[b] Jean-Louis Bantignies,[b] Olivier Cambon,[a] Gaëlle Creff,¶[e] Pascale Roy,[e] Jean-Blaise Brubach,[e] Tahar Hammouda,[f] Denis Andrault[f] and Julien Haines*[a]

Confined H_2O molecules act as local probes for depressurization phenomena during the pressure induced amorphisation of faujasite NaX at which the OH stretching frequency first decreases and then *increases* almost to its room pressure value upon further compression. Pair distribution function (PDF) analysis provides evidence that amorphisation corresponds to a collapse of the structure around hydrated sodium cations with strong distortion of the secondary building units (double six-membered rings, sodalite cages). Both the use of guest molecules as local probes in far- and mid-infrared spectroscopy, where we correlate intermolecular water H bonding vibrations and internal mode behaviour under confinement, and PDF analysis could be of great use to study the mechanical behaviour of other hydrated materials.

Introduction

Zeolites are of great interest due to their many applications, for instance, as catalysts and molecular sieves. Zeolites, due to their high porosity, exhibit interesting properties under pressure such as guest insertion[1–5] and amorphisation.[3,6–12] These may give rise to novel technological applications in the field of the absorption of mechanical energy (molecular springs, shock wave absorbers). In certain cases, the amorphisation process and densification of the amorphous forms can give rise to local depressurization effects,[9–12] which can be linked to the absorption of mechanical energy.

Faujasite NaX is a hydrated, X-type (corresponding to Si:Al = 1–1.5) sodium aluminosilicate zeolite with a cubic structure (space group $Fd\bar{3}m$ – O_h^7) built up of sodalite cages linked by double six-membered rings (D6MR) of TO_4 (T = Si, Al) tetrahedra.[13] The faujasite structure exhibits large voids, termed supercages, with a diameter of about 13 Å. Thus, this microporous mineral has one of the largest channel diameters and one of the largest void volumes of all natural zeolites. The hydrated, charge-compensating Na^+ cations are located in various sites in the three-dimensional pore network, including the large supercage.

Faujasite has been found to undergo pressure-induced amorphisation (PIA) at close to 2 GPa, by infrared[8] and Raman spectroscopy[10] and X-ray diffraction.[3,7,9,10] A further change from a low-density amorphous (LDA) to a high-density amorphous (HDA) form occurs in the pressure range between 2 and 4 GPa.[9,10,12] This phenomenon of polyamorphism is linked to local depressurization due to the significant volume change at the LDA–HDA transformation.

In the present work based on infrared spectroscopy, the hydrogen bonded water located inside the porous network can be used as a local probe to follow the changes occurring during pressure induced amorphisation and the LDA–HDA transformation. In addition, Raman spectroscopy along with X-ray total scattering with pair distribution function (PDF) analysis is used to obtain direct structural information on the recovered HDA form.

Experimental methods

Infrared spectroscopy

Faujasite NaX with a Si:Al ratio of 1.23 was obtained from SOMEZ (France). Mid infrared spectra (4000–400 cm^{-1}) were

[a] *Institut Charles Gerhardt Montpellier, UMR 5253 CNRS, Université Montpellier 2, 34095 Montpellier Cedex 5, France. E-mail: julien.haines@univ-montp2.fr*
[b] *Laboratoire Charles Coulomb, UMR 5221 CNRS-UM2, Département CVN, Université Montpellier 2, 34095 Montpellier Cedex 5, France*
[c] *CEA, DAM Le Ripault, 37260 Monts, France*
[d] *Research & Utilization Division, Japan Synchrotron Radiation Research Institute (JASRI, SPring-8), 1-1-1 Kouto, Sayo-cho, Sayo-gun, Hyogo 679-5198, Japan*
[e] *Synchrotron Soleil, L'Orme les Merisiers, Saint Aubin – BP48, 91192 Gif sur Yvette, France*
[f] *Laboratoire Magmas et Volcans, UMR CNRS 6524, Université Blaise Pascal, 63038 Clermont-Ferrand Cedex, France*
† Present address: Universidade de Caxias do Sul, Centro de Ciências Exatas e Tecnologia, 95070-560 Caxias do Sul, RS, Brazil.
‡ Present address: Synchrotron Soleil, L'Orme les Merisiers, Saint Aubin – BP48, 91192 Gif sur Yvette, France.
§ Present address: IPGP, Université Paris Diderot, 75005 Paris, France.
¶ Present address: Institut de Chimie de Nice, Université de Nice, 06108 Nice cedex 2, France.

recorded on a Bruker instrument IFS66v/s Fourier transform infrared spectrometer (FT-IR) equipped with mercury cadmium telluride – MCT (5000–750 cm^{-1}) and deuterated triglycine sulphate – DTGS (4000–400 cm^{-1}) detectors, KBr beamsplitter and a black body source. The far infrared measurements (30–400 cm^{-1}) were performed at the AILES beam line (synchrotron SOLEIL) equipped with a Bruker instrument IFS 55 FT-IR spectrometer modified to operate with the synchrotron source. The use of the synchrotron, with its much high brilliance in the far-infrared than a laboratory source, provides a better signal to noise ratio for the study of the very small samples under high-pressure. This spectral domain was investigated using a Si beamsplitter and a bolometer detector. The spectra were recorded with a resolution of 2 cm^{-1} with 400 scans (Far IR) and 128 (MCT) – 2048 (DTGS) scans (mid IR) per spectrum. A double condenser system (Cassegrain objectives, numerical aperture. 0.4) and a diamond anvil cell were used for the pressure experiments.

The gasket thickness and hole diameter were 50–60 μm and 140 μm, respectively, for the mid-IR and 30–50 μm and 300 μm, respectively, for the far-IR. The pressure transmitting medium and calibrant was NaBr:$NaNO_2$ (0.4%)[14,15] for the mid-IR and polyethylene and ruby,[16] respectively, for the far-IR.

Multianvil apparatus

A Walker-type multi-anvil apparatus was used to prepare the amorphous faujasite NaX following the previously described procedure.[17] A powder sample was placed in a 2.7 mm long, 2.5 mm internal diameter gold capsule and was loaded in a 10 mm edge length MgO octahedral sample cell. The sample cell was placed between the eight tungsten carbide anvil cubes with 32 mm edge lengths and a truncated face of 4 mm edge length in contact with the octahedron. Preformed 5 × 2 mm gaskets were used. This assembly was then positioned between the outer six anvils of the 1000 tonne, split-cylinder, multi-anvil device. The pressure was increased to 20 GPa over a period of 3.5 h and this pressure was maintained for 1 hour. The sample was decompressed slowly over a period of 15 h.

Raman spectroscopy

Raman spectra (105–1500 cm^{-1}) were obtained using a Horiba Jobin-Yvon Labram Aramis spectrometer equipped with a single monochromator and a thermoelectric Peltier-cooled charge coupled device detector (CCD). The samples were placed on microscope slides under the 50× or 100× objectives of the Olympus microscope and studied in back-scattering geometry. A 473 nm diode laser was used for excitation with an edge filter cut-off beginning at 105 cm^{-1}. The acquisition time was 60 s and three acquisitions were performed on each sample.

X-ray total scattering

High energy X-ray total scattering data from the recovered amorphous sample were obtained using the two axis horizontal diffractometer built for liquid and glass samples on the bending magnet beam line BL04B2 at the SPring-8 synchrotron. A bent Si (220) monochromator fixed at a Bragg angle of 3° in the horizontal plane was used to obtain 61.6 keV X-rays. The sample was placed on a Kapton film in the incident X-ray beam. The intensity of the scattered X-rays was measured using a Ge detector. The pair distribution function was obtained in the form of the total correlation function[18] $T(r)$ by direct Fourier transformation of the total scattering data $S(Q)$ obtained up to a maximum Q of 25 $Å^{-1}$. The details of experiment and standard data analysis are described elsewhere.[19,20]

Results and discussion

Infrared spectroscopy at high pressure

Faujasite NaX was studied at high pressure by mid- and far-IR spectroscopy (Fig. 1–4). Group theory predicts that in the O_h^7 space group, the faujasite framework should exhibit 28 infrared triply-degenerate F_{1u} modes. The infrared modes of various faujasites have been assigned previously.[8,21] The wavenumbers of the framework modes below 1200 cm^{-1} (Fig. 1), such as the

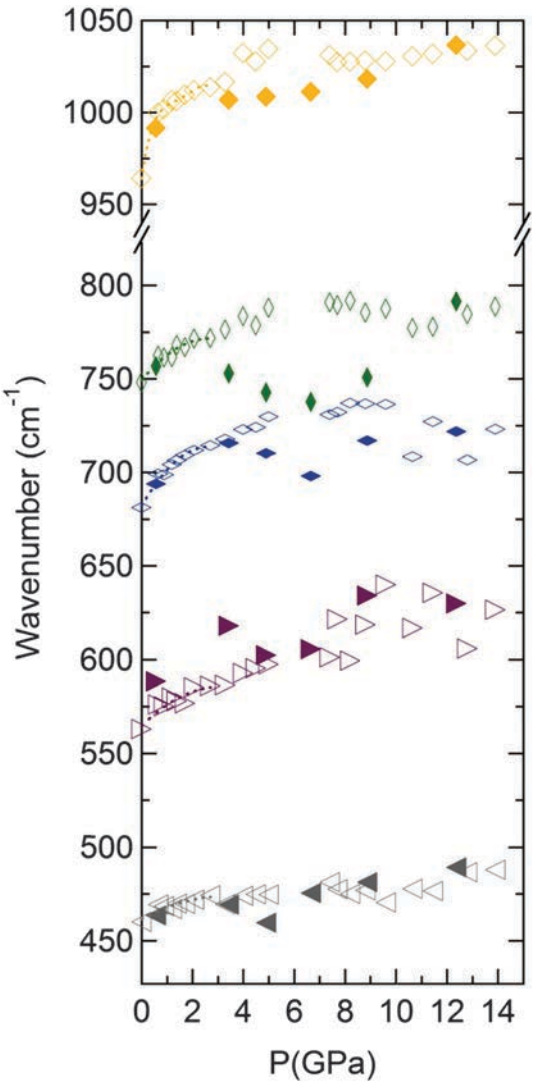

Fig. 1 Pressure dependence of the IR modes of the faujasite framework. Open and solid symbols correspond to points obtained upon compression and decompression, respectively.

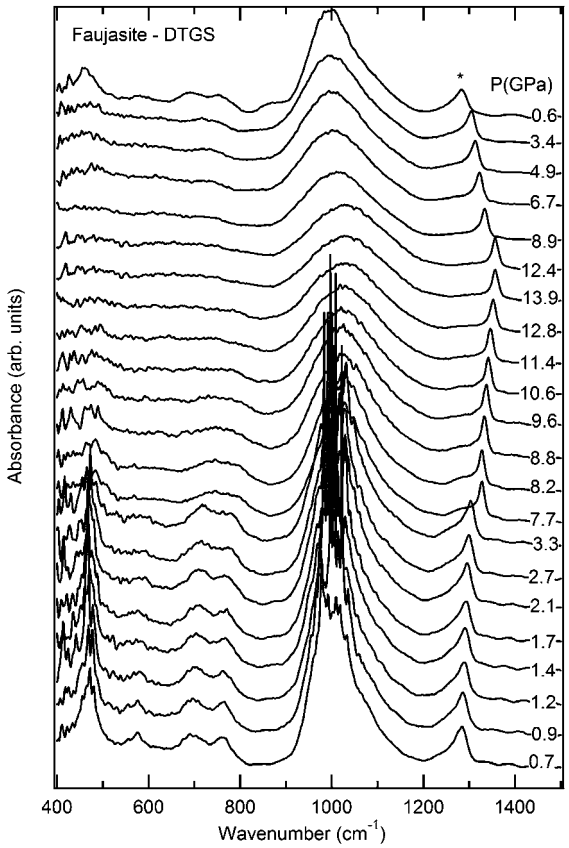

Fig. 2 Mid IR spectra in the region of the faujasite framework modes (DTGS detector) at selected pressures upon compression and upon decompression. The peak of the NO_2^- ion used as a pressure calibrant is indicated by an asterisk.

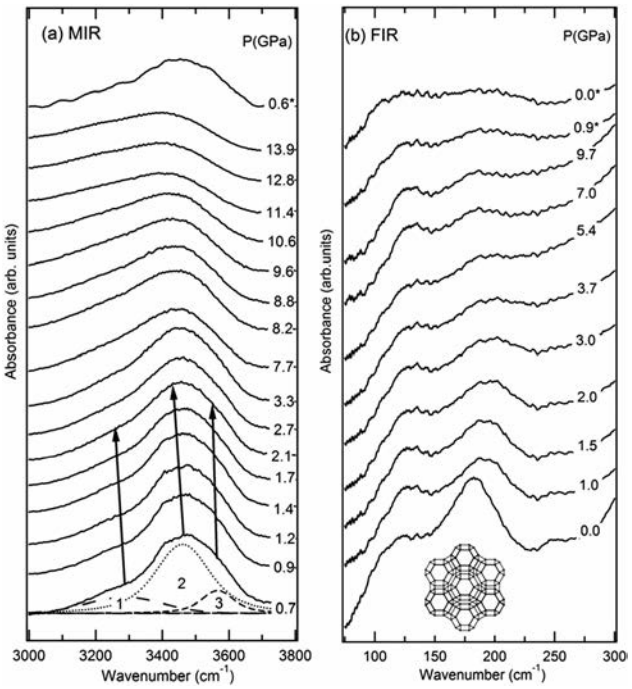

Fig. 3 (a) Mid (OH stretching region) and (b) far IR spectra of faujasite at selected pressures upon compression and upon decompression (*). Arrows indicate the initial shift of the three component bands. Inset: representation of the structure of faujasite showing the T-atom framework.

antisymmetric and symmetric O–T–O stretching modes (ν_{as}(OT)) and (ν_s(OT)) around 964 and 681 cm^{-1}, symmetric T–O–T stretching modes (ν_s(TO)) around 748 cm^{-1}, and the D6MR modes near 563 cm^{-1} initially strongly increase with pressure. The increase of the O–T–O deformation mode (δ(OT)) near 460 cm^{-1} is less marked. Band assignments are given in Table 1. A change in slope in the pressure dependence of the wavenumbers of the majority of modes is observed just below 2 GPa. This can be correlated to the strong decrease in crystallinity found in faujasite NaX by X-ray diffraction[10] particularly between 2 and 4 GPa, at which the intensities of the diffraction lines are typically less than 40% of their ambient pressure values. A major contribution to the change in slope can be expected to arise from the transformation from the initial crystalline state to the amorphous form, as above 2 GPa a significant amount of amorphous material is present. The IR bands of the amorphous form are in most cases slightly shifted to lower wavenumbers. The decrease and subsequent disappearance of the X-ray diffraction signal in faujasite, which then is replaced by a broad amorphous X-ray signal[10] indicates the progressive loss of long range order in the crystal.

Above 11 GPa, ν_s(TO) and ν_s(OT) cannot be differentiated anymore and a broad band around 753 cm^{-1} is observed. The weakening, followed by the gradual and almost complete disappearance of the mode near 574 cm^{-1} linked to the D6MR's is observed beginning from the onset of PIA near 1.5 GPa (Fig. 2). Some sharpening of the modes occurs upon decompression indicating that the presence of hydrated Na^+ cations in the pores may play a role in retaining a limited degree of medium-range order.

Due to the loss of X-ray diffraction signals resulting from the disappearance of long-range order upon PIA,[3,7,9,10] spectroscopic methods are extremely powerful to probe changes on a local level, especially by following the behaviour of molecules confined in the cages and channels of the porous structure. Below 2 GPa strong shifts in the three hydroxyl stretching components (ν(OH)) between 3200 and 3600 cm^{-1} (Fig. 3a, components 1, 2, 3) to lower wavenumbers are observed due to the strengthening of H-bonds and the weakening of the internal O–H bonds (Fig. 4). These three bands[22,23] are linked to tetrahedral H-bonds (around 3290 cm^{-1}), intermediate coordination environments (around 3460 cm^{-1}) and trimers, dimers and monomers (around 3590 cm^{-1}). Beginning at close to 2 GPa, a strong *increase* in the wavenumbers of these modes is observed, which with further increases in pressure reach values similar to those observed at room pressure providing clear evidence of local depressurization. Above 7 GPa, these bands begin to decrease in wavenumber and broaden with new features appearing at lower wavenumbers indicating wider distribution of hydrogen bonding environments for the confined water molecules.[26–28]

Intermolecular phonons due to H bonding (νHB) are directly probed in the far infrared between 100 and 200 cm^{-1} (Fig. 3b).[29–31] Two broad H bonding vibrational features are observed at ambient

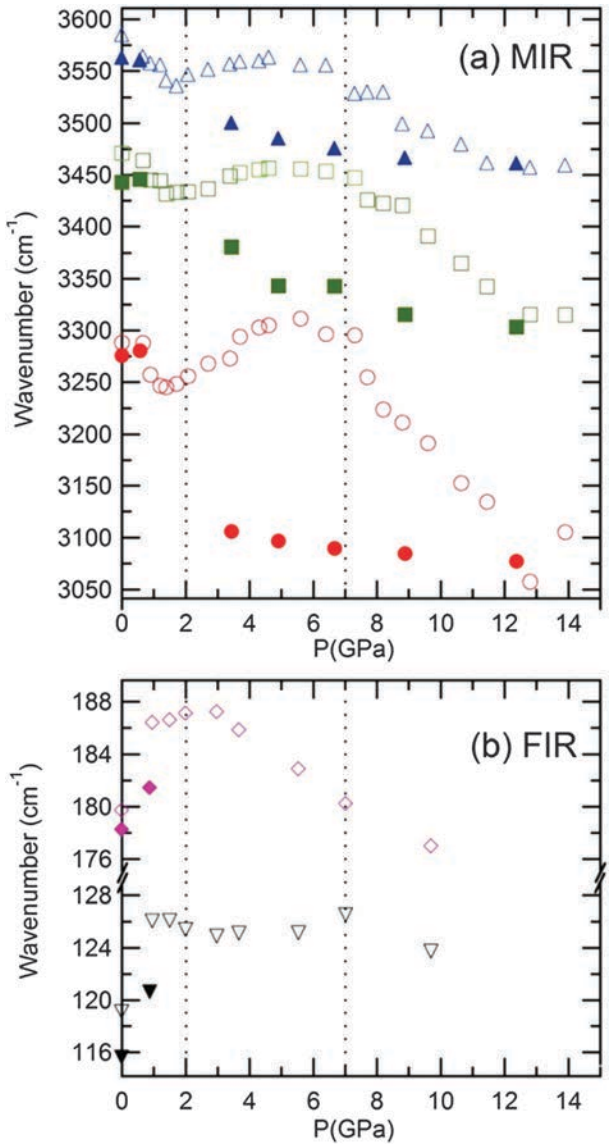

Fig. 4 Pressure dependence of the IR bands (OH and H-bond stretching regions) of faujasite. Open and solid symbols correspond to points obtained upon compression and decompression, respectively.

Table 1 Band assignments for faujasite NaX[21–25]

Wavenumber (cm^{-1})	Assignment
3590	O–H stretch trimers, dimers, monomers
3460	O–H stretch intermediate coordination
3290	O–H stretch tetrahedral H bonds
964	Antisymmetric O–T–O stretching
748	Symmetric T–O–T stretching
681	Symmetric O–T–O stretching
563	D6MR's
460	O–T–O deformation
180	HBa + Na^+ (S_{II}) translations
118	HBb + Na^+ ($S_{I'}$) translations

pressure around 180 and 118 cm^{-1} termed νHBa and νHBb in the following. Na^+ cation vibrations are also observed in this region. In dehydrated NaX,[24,25] sharp modes of Na^+ cations in S_{II} sites (supercage) and $S_{I'}$ sites (sodalite cage) are observed at 189 and 110 cm^{-1}, respectively. In hydrated NaX, coupling could be expected to occur between the translations of the hydrated Na^+ cations and stretching of the H bonds. In the hydrated material, the bands in this region are much broader and the relative intensity of the lower frequency band with respect to the higher frequency band is significantly higher. Progressive weakening and broadening of the external features νHB with the pressure increase is observed. The wavenumber shift as a function of pressure of the νHB features shows an upshift up to 2 GPa due to the strengthening of the hydrogen bonding. The higher frequency component νHBa, corresponding to the stronger H-bonds, is more affected and is discussed below. At this point, a major change in the trend is observed and the νHB intermolecular modes begin to decrease in frequency as a function of pressure due to the weakening of the hydrogen bonding. Significant changes occur in the region between 3.5 and 7 GPa, with the νHBa frequency almost returning to its room pressure value (Fig. 4). This is again clear evidence for local depressurization at the LDA–HDA transformation. At 9.7 GPa, a broad band is present corresponding to a large distribution of H bonding in agreement with the ν(OH) behaviour.

At higher pressure, collapse of the structure occurs producing the HDA form. From this point onward the frequencies of the intermolecular H bonding modes decrease due to the broad distribution of H-bonds in the collapsed structure. Upon pressure release, the H bonding features (internal modes νOH and external modes νHB) broaden, but due to the more compact arrangement and the large distribution of hydrogen bonds, νOH is always found at lower frequencies with respect to those obtained upon compression. Upon full pressure release, νOH appears typically at about 20 cm^{-1} lower than in the starting material. In the frequency region below 1200 cm^{-1}, the HDA form is also characterized by broadened bands occurring at slightly different frequencies with respect to the crystalline phase (Fig. 1). The bands linked to the D6MR's at 582 cm^{-1}, the sodalite cages at 461 cm^{-1} and pore opening (365 cm^{-1})[21] are particularly affected.

Study of the recovered HDA form by Raman spectroscopy and X-ray total scattering

In order to obtain direct structural information on the HDA form, a macroscopic sample was prepared in a multianvil device at 20 GPa. This sample was studied by X-ray total scattering and Raman spectroscopy. The Raman spectrum of the HDA form (Fig. 5) is characterized by broad bands and is similar to the Raman spectrum of pressure amorphized zeolites[10,11] and densified silica glass.[32–34] The low-frequency vibrations below 400 cm^{-1} of the faujasite framework are absent and two strong T–O–T bending vibrations between 400 and 600 cm^{-1} linked to highly strained T–O–T angles[11] and/or 3 or 4-membered rings[35] are present. These results indicate that major changes in the medium range order occur with PIA, which are also at the origin of the broad distribution of hydrogen bond environments probed *in situ* by infrared spectroscopy.

The X-ray total scattering data obtained for the HDA form of faujasite in the present work (Fig. 6) correspond to the typical X-ray scattering data obtained from an amorphous material

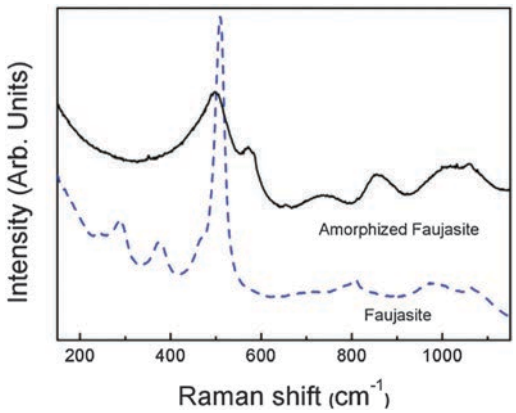

Fig. 5 Raman spectra of faujasite and pressure amorphized faujasite.

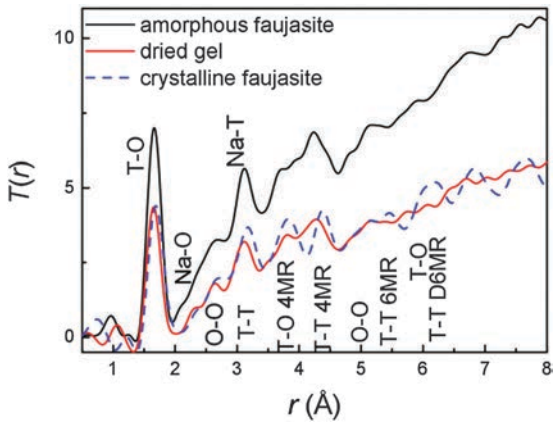

Fig. 7 Total correlation functions $T(r)$ of pressure-amorphised faujasite (this work), crystalline faujasite[36] and the dried gel used to prepare faujasite.[36]

and bear some similarities with those of the dried amorphous precursor gel[36] corresponding to the first step in the synthesis of faujasite. These data directly confirm that faujasite transforms to a fully amorphous material upon compression with the disappearance of the Bragg reflections of the initial crystalline phase (Fig. 6). The total correlation function data obtained from X-ray total scattering from the HDA form show broader features than that obtained from the crystalline form due to wider distributions of most interatomic distances and angles in the disordered amorphous material. These data also bear some similarities to those of the dried amorphous gel (Fig. 7); however, there are important differences linked to the densification process and the presence of H_2O. The recovered HDA form with a density of 2.5 g cm^{-3} is 41% more dense than the crystalline starting material. The average intratetrahedral T–O distances are essentially identical (1.65 Å-dried gel, 1.66 Å-faujasite[13] and HDA). Certain distance distributions are broader and shifted to longer distances in HDA with respect to the dried gel such as the Na–O distances and the O–O distances due to the presence of hydrogen bonded H_2O molecules. The T–T distances corresponding to the intertetrahedral T–O–T bridging angle are lower in the HDA form and the dried gel with respect to crystalline faujasite indicating a closure of the T–O–T angle.

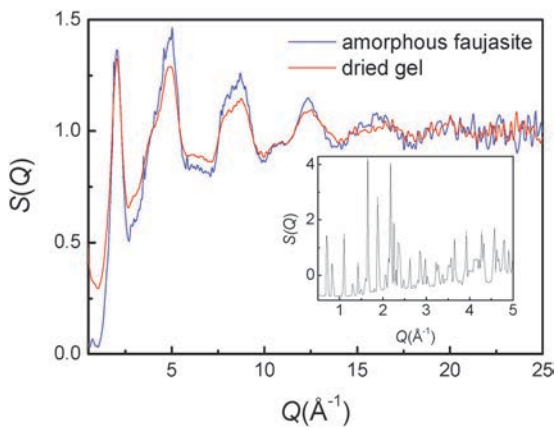

Fig. 6 Total scattering structure factor $S(Q)$ of pressure-amorphised faujasite (this work) and the dried gel used to prepare faujasite[36] as a function of X-ray scattering vector Q; $Q = (4\pi/\lambda)\sin\theta$. Inset: low Q region of the diffraction pattern of crystalline faujasite.[36]

The intertetrahedral T–O, T–T and O–O distances distributions (3.7–8 Å) are also significantly different and broadened due to the collapse of the framework. In certain cases, such as for the T–O distributions corresponding to the 4 membered rings (MR) the distribution has two maxima indicating a strong distortion of the 4MR's. It should be noted that one half of the 4MR's belongs to the sodalite cages and the other half belongs to the D6MR's. A strong maximum is observed at 4.23 Å in HDA, which is lower than 4.29 and 4.39 Å, corresponding to T–O (6MR) and T–T 4MR distributions in crystalline faujasite, indicating a strong distortion of these rings. Strong maxima linked to Si–O (6MR) are also observed in pressure-amorphized silicalite[11] and silica glass in this region.[37] There is a shoulder at 4.47 Å in HDA corresponding to a second diagonal distance in the distorted 4MR's. There is no evidence for the formation of 3MR's or additional 4MR's. Based on the present results the two strong T–O–T vibrations in the Raman spectrum can be linked to highly strained T–O–T angles as previously observed for silicalite[11] rather than an increase in the number of smaller rings. The O–O distances near 5 Å are similar in all three materials; however the T–T (6MR) distance (5.45 Å) decreases and the distribution broadens. All the distance distributions above 6 Å corresponding to the secondary building units (SBU), the D6MR's and the sodalite cages, are replaced by weak broad features indicating that amorphisation results in strong distortions to these units. These total X-ray scattering results allow us to identify the structural changes that occur upon amorphisation, which give rise to the short range order changes probed *in situ* by infrared spectroscopy. As the water molecules occupy the different SBU's and the supercages, which are built up of these SBU's, the strong distortion of such units in the amorphous form increases the distribution of different local environments available for the H_2O molecules as compared to the initial high-symmetry cubic faujasite structure resulting in the very broad distribution of hydrogen bonds and the broad OH bands in the infrared spectra. The decrease in certain distances and the observed distortions are responsible for the strong decrease in volume

upon pressure-induced amorphisation, which gives rise to the local depressurisation probed by the H_2O molecules in the high-pressure infrared experiment. The observed distortions of the different ring and cage structures and the broadening of the various distance distributions in the amorphous form also provide an explanation for the changes observed in the framework modes in the infrared spectra, in particular the disappearance of the 563 cm^{-1} mode linked to the D6MR, which is replaced by a broad feature after decompression and the broadening of the T–O stretching and O–T–O deformation modes.

The observed structural changes upon amorphisation in faujasite are consistent with a recent study on zeolite NaA; PDF analysis[38] showed that amorphisation was related to distortion in that case of the D4R's linking the sodalite cages and the simultaneous loss in regularity of the latter. In a recent study of a pressure-amorphized, sodalite-type metal organic framework containing I_2 molecules,[39] PDF results indicate that the sodalite topology is retained, but that the 6-membered rings are distorted. This type of collapse upon amorphisation, while retaining the topology of the starting material, was also observed for silicalite,[11] which has empty pores. Partial filling of the pores can be expected to favour the retention of the initial topology.

Conclusion

The present infrared results show that H_2O molecules act as local probes for the local depressurization occurring during the amorphisation process and the strong volume decrease occurring at the formation of the HDA form in faujasite. In particular, the OH stretching modes after initially decreasing due to strengthening of the hydrogen bonds then *increase* almost to their ambient pressure values over the pressure range between 2 and 4 GPa. This pressure range corresponds to that in which the intensities of the X-ray diffraction lines showed a very strong decrease due to pressure-induced amorphisation.[10] In the present study PDF analysis of the total X-ray scattering data provides direct structural information on the changes due to pressure-induced amorphisation, which can be correlated to the changes in the local environment of the H_2O molecules probed by infrared spectroscopy. The changes in interatomic distances and the width or the various distance distributions in the PDF provide evidence that amorphisation corresponds to a collapse of the structure around hydrated sodium cations with strong distortion of the SBU's (D6MR's, sodalite cages). The use of guest molecules as local probes in IR spectroscopy and PDF analysis could be of great use to study amorphisation in other porous materials.

Acknowledgements

We would like to thank David A. Keen (ISIS Facility) for useful discussions and David Bourgogne (ICGM) for technical assistance. We acknowledge the French National Research Agency (ANR) for funding through the research project ANR-09-BLAN-0018-01. The synchrotron radiation experiments were performed at the BL04B2 in the SPring-8 with the approval of the Japan Synchrotron Radiation Research Institute (JASRI) (Proposal Number 2008A1965). The multianvil apparatus of the Laboratoire Magmas et Volcans is financially supported by the Centre National de la Recherche Scientifique (Instrument National de l'INSU).

Notes and references

1 R. M. Hazen, *Science*, 1983, **219**, 1065–1067.
2 V. Eroshenko, R. C. Regis, M. Soulard and J. Patarin, *J. Am. Chem. Soc.*, 2001, **123**, 8129–8130.
3 M. Colligan, P. M. Forster, A. K. Cheetham, Y. Lee, T. Vogt and J. A. Hriljac, *J. Am. Chem. Soc.*, 2004, **126**, 12015–12022.
4 J. Haines, O. Cambon, C. Levelut, M. Santoro, F. Gorelli and G. Garbarino, *J. Am. Chem. Soc.*, 2010, **132**, 8860–8861.
5 B. Coasne, J. Haines, C. Levelut, O. Cambon, M. Santoro, F. Gorelli and G. Garbarino, *Phys. Chem. Chem. Phys.*, 2011, **13**, 20096–20099.
6 P. Gillet, J. M. Malezieux and J. P. Itie, *Am. Mineral.*, 1996, **81**, 651–657.
7 H. J. Liu, R. A. Secco and Y. N. Huang, *PhysChemComm*, 2001, **4**, 37–39.
8 E. A. Havenga, Y. N. Huang and R. A. Secco, *Mater. Res. Bull.*, 2003, **38**, 381–387.
9 G. N. Greaves, F. Meneau, A. Sapelkin, L. M. Colyer, I. A. Gwynn, S. Wade and G. Sankar, *Nat. Mater.*, 2003, **2**, 622–629.
10 A. Isambert, E. Angot, P. Hebert, J. Haines, C. Levelut, R. Le Parc, Y. Ohishi, S. Kohara and D. A. Keen, *J. Mater. Chem.*, 2008, **18**, 5746–5752.
11 J. Haines, C. Levelut, A. Isambert, P. Hebert, S. Kohara, D. A. Keen, T. Hammouda and D. Andrault, *J. Am. Chem. Soc.*, 2009, **131**, 12333–12338.
12 N. Greaves and F. Meneau, *J. Phys.: Condens. Matter*, 2004, **16**, S3459–S3472.
13 F. Busch, N. Jaeger, G. SchulzEkloff, R. Schnell, H. Klein and H. Fuess, *Zeolites*, 1996, **17**, 244–249.
14 D. D. Klug and E. Whalley, *Rev. Sci. Instrum.*, 1983, **54**, 1205–1208.
15 M. Ceppatelli, M. Santoro, R. Bini and V. Schettino, *J. Chem. Phys.*, 2000, **113**, 5991–6000.
16 H. K. Mao, J. Xu and P. M. Bell, *J. Geophys. Res.: Solid Earth*, 1986, **91**, 4673–4676.
17 T. Hammouda, *Earth Planet. Sci. Lett.*, 2003, **214**, 357–368.
18 D. A. Keen, *J. Appl. Crystallogr.*, 2001, **34**, 172–177.
19 M. Isshiki, Y. Ohishi, S. Goto, K. Takeshita and T. Ishikawa, *Nucl. Instrum. Methods Phys. Res., Sect. A*, 2001, **467**, 663–666.
20 S. Kohara, M. Itou, K. Suzuya, Y. Inamura, Y. Sakurai, Y. Ohishi and M. Takata, *J. Phys.: Condens. Matter*, 2007, **19**, 506101.
21 E. M. Flanigen, H. Khatami and H. A. Szymanski, *Adv. Chem.*, 1971, **101**, 201–229.
22 V. Crupi, D. Majolino, P. Migliardo, V. Venuti and U. Wanderlingh, *Eur. Phys. J. E: Soft Matter Biol. Phys.*, 2003, **12**, S55–S58.
23 J. B. Brubach, A. Mermet, A. Filabozzi, A. Gerschel and P. Roy, *J. Chem. Phys.*, 2005, **122**, 184509.

24 W. M. Butler, C. L. Angell, W. McAllister and W. M. Risen, *J. Phys. Chem.*, 1977, **81**, 2061–2068.
25 C. Peuker and D. Kunath, *J. Chem. Soc., Faraday Trans. 1*, 1981, **77**, 2079–2085.
26 J. L. Bantignies, L. Vellutini, J. L. Sauvajol, D. Maurin, M. W. C. Man, P. Dieudonne and J. J. E. Moreau, *J. Non-Cryst. Solids*, 2004, **345**, 605–609.
27 J. L. Bantignies, C. C. D. Moulin and H. Dexpert, *J. Pet. Sci. Eng.*, 1998, **20**, 233–237.
28 J. L. Bantignies, J. L. Sauvajol, A. Rahmani and E. Flahaut, *Phys. Rev. B: Condens. Matter Mater. Phys.*, 2006, **74**, 184509.
29 R. Bauer and G. Zundel, *J. Phys. Chem. A*, 2002, **106**, 5828–5831.
30 G. Creff, B. P. Pichon, C. Blanc, D. Maurin, J.-L. Sauvajol, C. Carcel, J. J. E. Moreau, P. Roy, J. R. Bartlett, M. Wong Chi Man and J.-L. Bantignies, *Langmuir*, 2013, **29**, 5581–5588.
31 J. L. Bantignies, S. Deabate, A. Righi, S. Rols, P. Hermet, J. L. Sauvajol and F. Henn, *J. Phys. Chem. C*, 2008, **112**, 2193–2201.
32 P. McMillan, B. Piriou and R. Couty, *J. Chem. Phys.*, 1984, **81**, 4234–4236.
33 R. J. Hemley, H. K. Mao, P. M. Bell and B. O. Mysen, *Phys. Rev. Lett.*, 1986, **57**, 747–750.
34 S. Sugai, H. Sotokawa, D. Kyokane and A. Onodera, *Physica B*, 1996, **219–220**, 293–295.
35 F. L. Galeener, R. A. Barrio, E. Martinez and R. J. Elliott, *Phys. Rev. Lett.*, 1984, **53**, 2429–2432.
36 T. Wakihara, S. Kohara, G. Sankar, S. Saito, M. Sanchez-Sanchez, A. R. Overweg, W. Fan, M. Ogura and T. Okubo, *Phys. Chem. Chem. Phys.*, 2006, **8**, 224–227.
37 M. G. Tucker, D. A. Keen, M. T. Dove and K. Trachenko, *J. Phys.: Condens. Matter*, 2005, **17**, S67–S75.
38 J. E. Readman, P. M. Forster, K. W. Chapman, P. J. Chupas, J. B. Parise and J. A. Hriljac, *Chem. Commun.*, 2009, 3383–3385.
39 K. W. Chapman, D. F. Sava, G. J. Halder, P. J. Chupas and T. M. Nenoff, *J. Am. Chem. Soc.*, 2011, **133**, 18583–18585.